Experimental Investigation of Hydrodynamic Response of an Ocean Uranium Extraction Machine Attached to a Floating Wind Turbine

Citation: Haji, Maha N. et al. "Experimental Investigation of Hydrodynamic Response of an Ocean Uranium Extraction Machine Attached to a Floating Wind Turbine." International Journal of Offshore and Polar Engineering 28, 3 (September 2018): 225–231. © 2018 International Society of Offshore and Polar Engineers

Published Version: http://dx.doi.org/10.17736/ijope.2018.jc735

Publisher: International Society of Offshore and Polar Engineers

Permanent Link: https://hdl.handle.net/1721.1/123823

Version: Author's final manuscript: final author's manuscript post peer review, without publisher's formatting or copy editing

Experimental Investigation of Hydrodynamic Response of a Symbiotic Machine for Ocean Uranium Extraction combined with a Floating Wind Turbine

Maha N. Haji, Jocelyn M. Kluger, Justin W. Carrus, Themistoklis P. Sapsis, and Alexander H. Slocum
Department of Mechanical Engineering, Massachusetts Institute of Technology
Cambridge, MA, USA

ABSTRACT

Developing methods to cost-effectively harvest uranium from seawater, which is estimated to contain 1000 times more uranium than on land, are crucial to the continued viability of nuclear power generation given that conventional sources of uranium are forecast to be depleted within a century. Studies have shown that coupling a uranium harvester system with an existing offshore structure, such as a wind turbine, could greatly reduce the cost of harvesting uranium from seawater as it eliminates the need for dedicated moorings and increases the overall energy-gathering ability of an offshore wind farm. This paper explores the hydrodynamic effects of adding a uranium harvester to an offshore floating wind turbine. The experimentally determined hydrodynamic responses of two designs of a Symbiotic Machine for Ocean uRanium Extraction (SMORE) are compared with that of an unmodified floating wind turbine (FWT). Both SMORE designs utilize adsorbent filament that is enclosed in a hard permeable shell to decouple the mechanical and chemical requirements of the device. It was found that both SMORE designs do not significantly shift the resonant peaks of the FWT.

KEY WORDS: Seawater uranium; offshore floating wind turbine; uranium adsorption; design; hydrodynamics; experiment; prototype.

INTRODUCTION

With global conventional terrestrial reserves of uranium (estimated at 7.6 million tonnes) expected to be depleted in a little over a century (OECD, 2016), it is expected that future uranium supplies will come from lower quality sites, resulting in higher extraction costs and even greater environmental impact. Fortunately, approximately 4.5 billion tonnes of uranium exist in the worlds oceans (Tamada, 2009) in concentrations of about 3 ppb (Oguma et al., 2011). It has been found that the most promising method of recovering uranium from seawater is through the use of chelating polymers (Kim et al., 2013). In this method, chelating polymers are deployed in seawater and remain submerged until the amount of captured uranium approaches the adsorption capacity. The polymer is then run through an elution bath to strip off uranium and other metal ions. The polymer may be immersed several times in elution baths before it needs to be regenerated by an alkali wash to free its functional groups, allowing for the reuse of the polymer. The output from the elution process undergoes purification and precipitation typical for mined uranium to produce yellowcake.

Initial concepts for offshore systems for the extraction of uranium from seawater utilized an adsorbent that is deployed and moored for extended periods of time, brought back to shore for the elution process, and redeployed afterward. These stand-alone, intermittent operation systems have been shown to have significant practical and economic deployment challenges (Seko et al., 2003) and to date none of these systems have been found to be economically viable. Specifically, detailed economic analysis by Schneider and Sachde (2013) found that a major cost driver of seawater uranium extraction is the mooring and recovery of the adsorbent. The Symbiotic Machine for Ocean uRanium Extraction (SMORE) described in this paper aims to reduce these mooring and deployment costs by developing a system that is attached to an offshore wind turbine and continuously takes the adsorbent from the ocean through an elution process and then returns it to the ocean. The integration of a uranium harvesting system with an offshore wind turbine tower is pursued be- cause the systems can then share structural support and moorings, which reduces their cost compared to standalone systems (Byers et al., 2016).

SMORE utilizes the structure of a offshore floating wind turbine (FWT) to provide the mooring and structural support for an autonomous, offshore uranium harvesting platform. SMORE is sized to recover 1.2 tonnes of uranium from seawater per year, enough annual fuel for 5-MW worth of nuclear power (Haji and Slocum, 2016) and is designed to work with the National Renewable Energy Laboratory (NREL) 5-MW wind turbine mounted on the OC3-Hywind floating spar (Jonkman et al., 2009; Jonkman, 2010). Thus about 200 FWTs would also provide enough yellowcake to manufacture fuel for a 1 GW nuclear power plant. It is important to ensure that the addition of the uranium harvester to the FWT will not adversely affect the dynamics of the FWT, which could result in reduced power output by the turbine, increased material requirements for the turbine, or changes in the turbine's operation and maintenance. FWT motion complicates rotor aerodynamics and control, which gen-

erally decreases FWT efficiency, and increases FWT structural stresses (Sebastian and Lackner, 2013; Tran and Kim, 2015; Jonkman and Matha, 2009; Kluger et al., 2017). This paper experimentally investigates the hydrodynamic responses of full-scale SMORE designs and compares the responses to that of an unmodified NREL 5-MW OC3-Hywind floating spar wind turbine.

THEORY

The hydrodynamics of the floating spar buoy wind turbine are considered in head-on incident waves of amplitude A and frequency ω which result in heave, X_3, and coupled surge, X_1, and pitch, X_5, degrees of freedom taken about the still water line (SWL) (as shown in figure 1).
The linear equations of motion of the system are given by

$$(\mathbf{M} + \mathbf{A})\ddot{\xi} + \mathbf{B}\dot{\xi} + \mathbf{C}\xi = \mathbf{X}(t), \tag{1}$$

where $\mathbf{M}$ is the mass matrix, $\mathbf{A}$ is the added mass coefficient matrix, $\mathbf{B}$ is the linear damping coefficient matrix, $\mathbf{C}$ is the restoring coefficient matrix, ξ is the platform displacement about the still waterline, and $\mathbf{X}$ is a matrix of the hydrodynamic excitation forces and moments.

Utilizing a linear frequency-domain analysis, the exciting forces and moments due to plane progressive waves will be assumed to be of the form,

$$X_j(t) = \Re\left\{\mathbb{X}_j(\omega)e^{i\omega t}\right\}, \quad \text{for } j = 1, \ldots, 6, \tag{2}$$

where j is the index for each degree of freedom and $\mathbb{X}_j(\omega)$ is a complex quantity. By virtue of linearity, the turbine's response to wave excitation will be of the form,

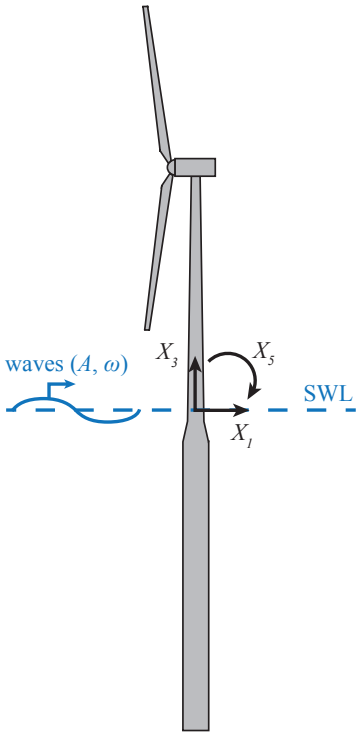

Fig. 1 Floating spar wind turbine, similar to that of the NREL 5-MW wind turbine mounted on the OC3-Hywind spar (Jonkman et al., 2009; Jonkman, 2010) with incident waves of amplitude A and frequency ω. The motions of the turbine are described about the still water line (SWL).

$$\xi_j(t) = \Re\left\{\Xi_j(\omega)e^{i\omega t}\right\}, \quad \text{for } j = 1, \ldots, 6, \tag{3}$$

where $\Xi_j(\omega)$ is a complex quantity. Combining (1)-(3) yields the following equations of motion in the frequency domain

$$\left[-\omega^2(M_{ij} + A_{ij}(\omega)) + i\omega B_{ij}(\omega) + C_{ij}\right]\Xi_j(\omega) = \mathbb{X}_i(\omega), \tag{4}$$

where Einstein notation is used for the cross-coupling terms in each equation of motion i.

The principal seakeeping quantity from a linear seakeeping analysis of a floating body at zero speed is the Response Amplitude Operator (RAO), defined as

$$RAO_j(\omega) = \left|\frac{\Xi_j(\omega)}{A/R^n}\right|, \tag{5}$$

where R is the turbine radius, $n = 0$ for $j = 1, 3, 5$ and $n = 1$ for $j = 2, 4, 6$.

For the case of an arbitrary shape such as an offshore wind turbine, it is common practice to examine the dynamic response numerically. Jonkman (2010) conducted a numerical study of the hydrodynamic response of the NREL 5-MW OC3-Hywind floating spar wind turbine using the WAMIT computer program (Newman and Sclavounos, 1988; Lee and Newman, 2010). This program uses a three-dimensional numerical-panel method in the frequency domain to solve response of the turbine to linear wave forcing due to potential flow. The excitation force and RAOs determined by Jonkman (2010) will be compared to the results of the excitation forces and RAOs found in the experiment detailed in this paper.

EXPERIMENTAL SETUP

Model scaling

A 1:150 Froude scaled model of two different versions of SMORE and the NREL 5-MW OC3-Hywind floating spar wind turbine were developed for testing to determine both the wave excitation forces on the structure and the response of each design to the incoming waves. This experiment used a geometric scale, $\lambda = 150$, which is defined to be

$$\lambda = \frac{L_f}{L_m}, \tag{6}$$

where L_f is the full-scale characteristic length and L_m is the model scale characteristic length. Table 1 details the scale ratios for many of the physical parameters utilized in this experiment. For instance, while acceleration varies only by a ratio of 1 between the model and full scale, the force scales by a factor of λ^3 (Chakrabarti, 1994).

Models for testing

Two scaled designs of SMORE were developed for testing, in addition to a scale model of the unmodified floating spar wind turbine. The unmodified floating spar wind turbine was scaled from dimensions detailed by Jonkman, et al. (2009) and Jonkman (2010). Some of the key parameters and their full-scale and model values are detailed in table 2, as determined from Jonkman (2010) and Myhr et al. (2014).

The model scale reference floating wind turbine was fabricated using aluminum cylinders turned down to the diameters of the upper and lower

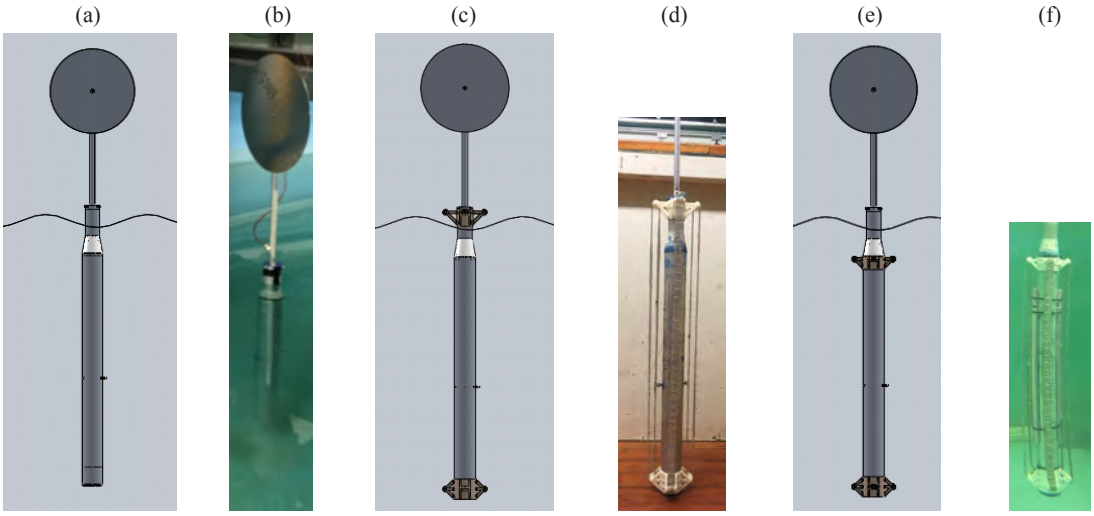

Fig. 2 Three-dimensional solid models and fabricated designs for the reference floating wind turbine, (a) and (b), the SMORE design with the upper platform out of the water, (c) and (d), and the SMORE design with the upper platform submerged, (e) and (f).

Table 1 Scaling ratios for various physical parameters

Variable	**Dimensions**	**Units**	**Scale Ratio**
Length	L	m	λ
Mass	M	kg	λ^3
Angle	none	rad	1
Acceleration	L/T^2	m/s^2	1
Angular Acceleration	1/T^2	1/s^2	λ^{-1}
Angular Velocity	1/T	1/s	$\lambda^{-0.5}$
Force	(M×L)/T^2	kg×m/s^2	λ^3
Wave Height	L	m	λ
Wave Period	T	m	$\sqrt{\lambda}$
Velocity	L/T	m/s	$\sqrt{\lambda}$
Moment of Inertia	M×L^2	kg×m^2	λ^5

Table 2 Scaling factors employed for wave model testing

Variable	**Unit**	**Full-Scale**	**Model Scale**
Total draft	m	120	0.8
Tower height	m	77.6	0.52
Depth to top of taper below SWL	m	4	0.027
Depth to bottom of taper below SWL	m	12	0.080
Diameter above taper	m	6.5	0.043
Diameter below taper	m	9.4	0.063
Platform mass	kg	1700000	0.5
Tower mass	kg	249718	0.074
Ballast	kg	5766000	1.71
CM location below SWL	m	89.92	0.60

turbine spar, an aluminum tube for the turbine tower, a circular plate to simulate the rotor damping on the turbine, and a transition region 3D printed from acrylonitrile butadiene styrene. All holes and joints were made waterproof using Permatex Sensor-Safe Blue RTV Silicone Gasket Maker.

The SMORE designs decouple the chemical and mechanical requirements of deploying the adsorbent in the rough ocean environment by using spherical shell enclosures to house the polymeric adsorbent (Haji et al., 2015). These shells are incrementally placed along high strength mooring rope, resembling conventional ball-chain belts. The lengths of shells are then connected together using cross-members of of high-strength marine grade rope to develop a net-like structure. These cross-members decrease the likelihood of tangling between ball-chain lengths and increase the rigidity of the overall component. The rope is then strung between a set of upper and lower rollers to move multiple ball-chain lengths through the water column (Haji and Slocum, 2016).

It was hypothesized that a SMORE design such as that described in Haji and Slocum (2016) in which an upper platform with the top rollers out of the water could have significant risks due to the wave loads near the surface. Given that wave energy decays exponentially with depth, placing the upper platform significantly underneath the water surface could be one way to mitigate these risks. Therefore, in addition to the unmodified floating spar wind turbine, two SMORE designs were tested. In the first design, the top set of rollers was placed out of the water at 0.03 m above the SWL (corresponding to 4.5 m in a full-scale design). In the second design, the top set of rollers was submerged 0.12 m below the SWL (corresponding to 18 m in a full-scale design). Figure 2 shows the three-dimensional models and fabricated designs used for testing.

The adsorbent ball-chain net was modeled using 3 mm diameter (#6 trade size) nickel-plated steel bead chain and the upper and bottom platforms of rollers were 3D printed out of acrylonitrile butadiene styrene. At every five beads, the chains were connected using a thermoplastic adhesive to mimic the increased rigidity that would be provided by rope cross-members of the ball-chain net. Because 3 mm diameter bead-chain was not available in plastic, the bead-chain net added more weight to the model than would be seen in the full-scale version. Therefore, strips of foam were added along the length of the turbine to increase its buoyancy and ensure it had a draft of approximately 0.8 m. The foam strips along the length of the turbine mimicked the additional buoyancy that plastic

shells with polymer adsorbents would provide to the overall structure. Additionally, the strips were added to the turbine in such a way as to limit the effects of the changed geometry on the turbine's hydrodynamic coefficients.

Experimental facilities

The tests described in this paper were conducted in the MIT Tow Tank, which is 30.5 m long, 2.1 m wide, and 1.2 m deep (100 ft long, 8 ft wide, and 4 ft deep). The wave maker at one end is a hydraulically driven vertical paddle with controllable amplitude and frequency that are controlled by LabView.

As shown in figure 3, two wave probes were used to measure the amplitude of the passing waves. One probe was located approximately 9.5 m (31 ft) downstream of the wave maker and another was located at mid-width in the tank 11.9 m (39.17 ft) downstream of the wave maker, closer to one of the walls of the tank. The models for testing were located about half-way down the length of the tank.

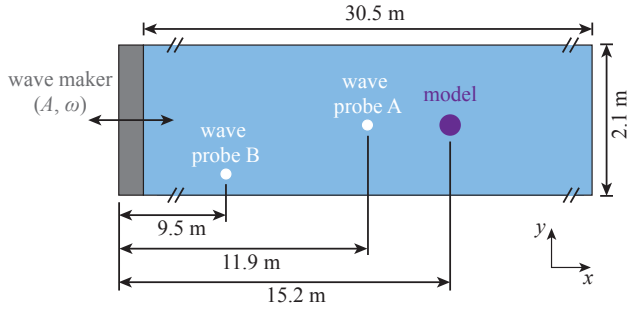

Fig. 3 Schematic of the experimental configuration. The wave maker on the left was excited at an amplitude, A, and frequency ω. Two wave probes (white dots) downstream measured the amplitude incoming to the model (purple) for all tests.

Excitation Forces

In order to measure the excitation forces on the designs, the models were constrained by a set of three load cells in the configuration shown in figure 4. All load cells were SMT Overload Protected S-Type Load Cells. The heave load cell was rated to 1.1 lbf (~ 4.9 N) and the top and bottom surge load cells were rated to 2.2 lbf (~ 9.79 N). Stinger rods measuring 24 mm and 12 mm connected the bottom and top surge, and heave load cell to the turbine tower, respectively. Each load cell was connected to a LabView data acquisition unit through a DC powered FUTEK amplifier module to increase the signal readings. The load cells were powered with a stacked dual power supply outputting ~20.7 V for all trials. The bottom surge load cell was approximately 0.057 m above the SWL and the top surge load cell was 0.24 m above the SWL. The surge force was taken to be the sum of the readings of the top and bottom load cells. The resulting pitch torque was determined by

$$X_5 = X_{1,top} z_{top} + X_{1,bottom} z_{bottom}, \tag{7}$$

where $X_{1,top}$ and $X_{1,bottom}$ are the top and bottom surge force load cell readings, respectively, and z_{top} and z_{bottom} are the distances of the load cells to the SWL, respectively.

In order to obtain frequency dependent data for both the wave excitation forces and response amplitude operators, the wave maker was excited at various frequencies and amplitudes for each model test. The wavemaker was programed to excite waves for 20 periods for all tests. Because the wave excitation force varies with frequency, ω, the load cell data were filtered using a Fast-Fourier Transform to obtain the amplitude of the forces at the frequency of interest.

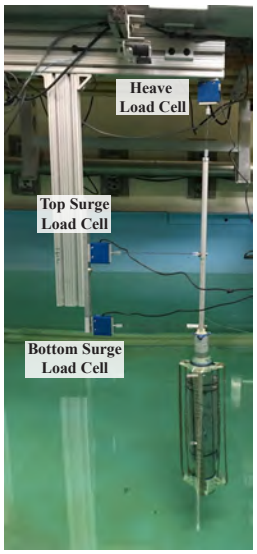

Fig. 4 Experimental setup of the excitation force test. One load cell was used to measure heave and two were used to measure surge. The difference in measurement of the two surge load cells and their distance from the SWL was used to determine the pitch torque.

Response Amplitude Operators

To determine the response amplitude operators of the models, tests were conducted in which the models were freely floating and an accelerometer mounted to the tower of the turbine measured heave, surge, and pitch motions. The accelerometer was a SparkFun 9 Degree of Freedom Sensor Stick. The accelerometer was configured to measure ± 2 g in acceleration and ± 245 deg/s in angular velocity using a Teensy 3.2 USB development board powered through a laptop USB port. The experimental setup is shown in figure 5.

Because the accelerometer was mounted above the SWL, the measurements had to be translated by

$$\mathbf{a}^{\mathrm{SWL}} = \mathbf{a}^{0} + \boldsymbol{\omega}^{\mathrm{T}} \times \left(\boldsymbol{\omega}^{\mathrm{T}} \times \mathbf{r}^{0,\mathrm{SWL}}\right) + \boldsymbol{\alpha}^{\mathrm{B}} \times \mathbf{r}^{0,\mathrm{SWL}}, \tag{8}$$

where $\mathbf{a}^{\mathrm{SWL}}$ is the acceleration of the turbine at the SWL, $\mathbf{a}^{0}$ is the acceleration of the turbine measured at the accelerometer, $\boldsymbol{\omega}^{\mathrm{T}}$ is the angular acceleration of the turbine as measured by the accelerometer, $\mathbf{r}^{0,\mathrm{SWL}}$ is the position vector from the location of the accelerometer to the SWL, and $\boldsymbol{\alpha}^{\mathrm{T}}$ is the angular acceleration of the turbine, as determined from the accelerometer. Note that because the turbine is assumed to be a rigid body, the angular velocity, $\boldsymbol{\omega}^{\mathrm{T}}$, and angular acceleration, $\boldsymbol{\alpha}^{\mathrm{T}}$ are the same at all points on the body.

In order to obtain frequency dependent data for the response amplitude operators, the wave maker was excited at various frequencies and amplitudes for each model test. The wavemaker was programed to excite waves for 20 periods for all tests. Given that the response amplitude operator is a function of frequency, ω, the acceleration and angular velocity data were filtered using a Fast-Fourier Transform to obtain the amplitude of the response at the frequency of interest.

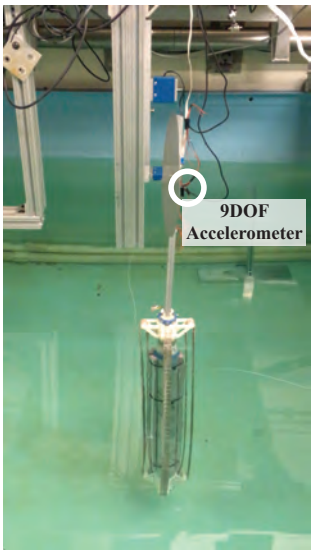

Fig. 5 Experimental setup of the RAO test. A 9DOF accelerometer mounted to the tower of the turbine was used to measure heave, surge, and pitch motions.

RESULTS

The results for the excitation force and RAOs for all models tested are shown and discussed in this section. All experimentally determined results are compared to the numerical results of the unmodified OC3-Hywind reference wind turbine (Jonkman, 2010).

Excitation Forces

Surge Excitation Force

Figure 6 shows the full-scale surge excitation force for the reference turbine, SMORE with the upper platform above the water, and SMORE with the upper platform submerged. In the case of the unmodified wind turbine, the surge excitation force is slightly increased as compared to the OC3-Hywind numerical results (Jonkman, 2010). This discrepancy could be due to slight differences in the model turbine's mass distribution properties as compared to Jonkman (2010). Although the magnitude of the surge excitation force is increased for the experimentally tested turbine as compared to those determined numerically, the trends are consistent between the experimentally and numerically determined surge excitation force. Additionally, there is good consistency in the normalized surge force for different wave amplitudes.

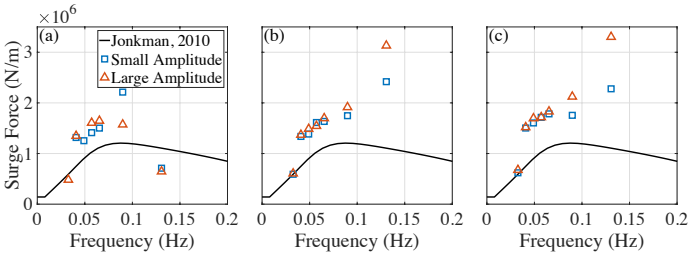

Fig. 6 Full-scale surge excitation force as determined by the load cell tests for small (blue squares) and large (red triangles) amplitude waves as compared to the OC3-Hywind numerical results (Jonkman, 2010)(black line) for the (a) reference floating wind turbine, (b) SMORE design with the upper platform above the water, and (c) SMORE design with the upper platform submerged.

For the case of SMORE with both the upper platform out of the water (figure 6b) and with the platform submerged (figure 6c), the surge excitation force has a similar magnitude to the experimental standalone reference floating wind turbine test (figure 6a). This suggests that the SMORE design with the upper platform above the water surface does not significantly affect the FWT surge excitation forces.

Heave Excitation Force

As seen in figure 7a, there is excellent agreement between the heave excitation force for the unmodified turbine as the OC3-Hywind numerical results (Jonkman, 2010) and experimentally measured by the load cells. The experimentally determined heave excitation force for the experimental SMORE system with the upper platform above the water (figure 7b) agrees well with the heave excitation force for the unmodified turbine. On the other hand, the heave excitation force of SMORE with the upper platform submerged (figure 7c) shows an increase in the full-scale heave excitation force compared to the unmodified turbine (figure 7a). This is expected because submerging the upper platform adds a significant amount of heave frontal area excited by waves. The heave natural frequency remains the same since the system waterplane area is unaffected and the SMORE heave mass and added mass is minimal compared to the FWT mass.

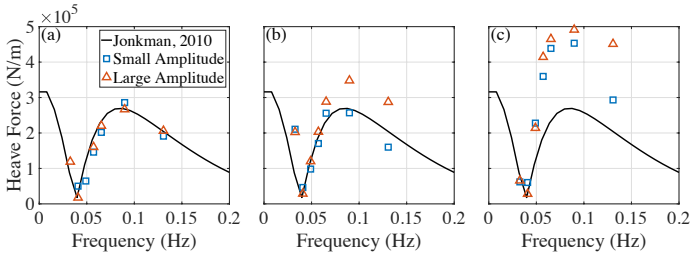

Fig. 7 Full-scale heave excitation force as determined by the load cell tests for small (blue squares) and large (red triangles) amplitude waves as compared to the OC3-Hywind numerical results (Jonkman, 2010) (black line) for the (a) reference floating wind turbine, (b) SMORE design with the upper platform above the water, and (c) SMORE design with the upper platform submerged.

Pitch Excitation Torque

Similar to the experimentally determined surge excitation force, the pitch excitation torque of the unmodified experimental floating wind turbine (figure 8a) is slightly increased as compared to that predicted by Jonkman (2010). Because the surge and pitch motions of a floating wind turbine are coupled, this discrepancy is likely due to the same reason the measured surge excitation force is larger than that predicted by the OC3-Hywind numerical results (Jonkman, 2010); and could be due to discrepancies between the model and experimental mass distributions. Although the magnitude of the pitch excitation torque is increased for the experimentally tested turbine as compared to that determined numerically, the trends are consistent between the experimentally and numerically determined pitch excitation torque.

Response Amplitude Operators

Surge RAO

For the unmodified floating wind turbine, the experimentally determined surge RAO (figure 9a) is slightly increased from the OC3-Hywind numerical results (Jonkman, 2010). The minimal differences in the surge

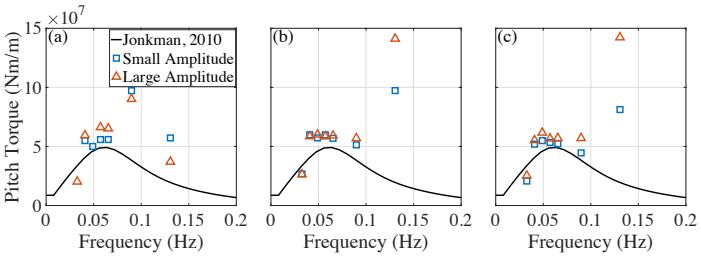

Fig. 8 Full-scale pitch excitation torque as determined by the load cell tests for small (blue squares) and large (red triangles) amplitude waves as compared to the OC3-Hywind numerical results (Jonkman, 2010) (black line) for the (a) reference floating wind turbine, (b) SMORE design with the upper platform above the water, and (c) SMORE design with the upper platform submerged.

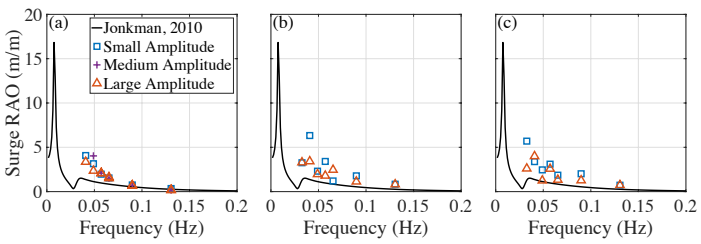

Fig. 9 Full-scale surge RAO as determined by the accelerometer tests for the (a) reference floating wind turbine, (b) SMORE with the upper platform above the water, and (c) SMORE with the upper platform submerged, for small (blue squares), medium (purple crosses) and large (red triangles) amplitude waves as compared to the OC3-Hywind numerical results (Jonkman, 2010) (black line).

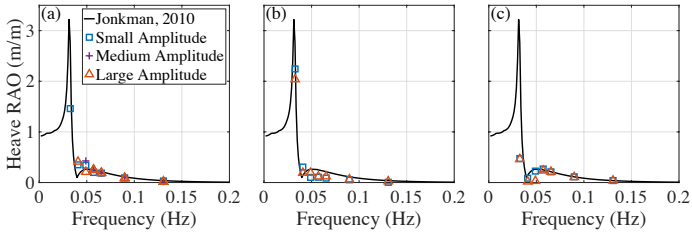

Fig. 10 Full-scale heave RAO as determined by the accelerometer tests for the (a) reference floating wind turbine, (b) SMORE with the upper platform above the water, and (c) SMORE with the upper platform submerged, for small (blue squares), medium (purple crosses) and large (red triangles) amplitude waves as compared to the OC3-Hywind numerical results (Jonkman, 2010) (black line).

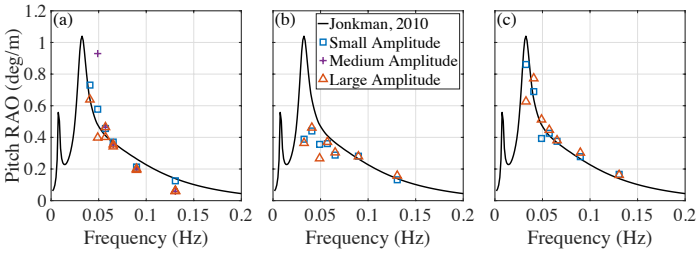

Fig. 11 Full-scale pitch RAO as determined by the accelerometer tests for the (a) reference floating wind turbine, (b) SMORE with the upper platform above the water, and (c) SMORE with the upper platform submerged, for small (blue squares), medium (purple crosses) and large (red triangles) amplitude waves as compared to the OC3-Hywind numerical results (Jonkman, 2010) (black line).

RAO may be due to the fact that the rotor on the model system was not able to be accurately scaled to match the same drag dynamics of the full size rotor. The surge RAO for both SMORE with the upper platform above the water (figure 9b) and SMORE with the upper platform submerged (figure 9c) show good agreement with the experimentally determined surge RAO for the unmodified turbine. This suggests that the surge response of the turbine is minimally affected by the addition of either SMORE design.

Heave RAO

In the case of the heave RAO, the unmodified floating wind turbine experimentally determined response agrees extremely well with the OC3-Hywind numerical results (Jonkman, 2010) (figure 10a). The SMORE design with the upper platform above the water also exhibits a similar heave response (figure 10b), suggesting the addition of this type of SMORE design does not affect the turbine's heave motion. On the other hand, the heave response is slightly decreased for the SMORE design with the upper platform submerged (figure 10c) from that determined by Jonkman (2010). This is likely due to the additional damping in heave provided by all of the submerged structures on the floating wind turbine.

Pitch RAO

As with the heave RAO, the unmodified wind turbine's measured pitch RAO (figure 11a) agrees well with the OC3-Hywind numerical results (Jonkman, 2010). The same is true for the pitch RAO for the SMORE design with the upper platform submerged (figure 11c), suggesting that this modification to the turbine does not affect its pitch motions. On the other hand, the upper platform above the water shows a decrease in the pitch response, especially near the pitch resonant frequency for the unmodified turbine (figure 11b). This is likely due to the additional roller platform near the bottom of the turbine which acts to increase the restoring pitch torque.

CONCLUSIONS AND CONTINUED WORK

The results of the model testing of various SMORE designs indicate that both designs, one in which the upper platform is out of the water and another in which it is submerged, have little effect on the overall hydrodynamics of the wind turbine platform to which the uranium harvester is attached. The SMORE design with an upper platform above the water somewhat reduced both the heave and pitch responses of the platform in most frequencies. While small, this beneficial effect may increase the FWT rotor efficiency and reduce stresses in the tower, and could contribute somewhat to a lower cost of energy for the wind power. Furthermore, the resonant frequencies of the turbine response are not significantly affected by the addition of either of the SMORE systems. This is key because an offshore wind turbine is tuned such that its resonant frequencies are in the range of 0.0077-0.0313 Hz, which are well below the significant ocean wave frequencies.

Although both SMORE designs do not significantly affect the dynamics of the turbine to which they are they are attached to, other considerations should be taken into account when determining the design of SMORE. Biofouling, which has been shown to have a detrimental effect on the

adsorbent's uranium extract capabilities (Park et al., 2016), could be mitigated by submerging the upper platform as that may reduce light and air contact with the adsorbent. Additionally, submerging the upper platform to below the ocean surface could greatly reduce wave loads on the uranium harvester given that wave forcing decreases exponentially with depth. On the other hand, designing a chemical system to extract uranium from the adsorbent for SMORE with a submerged upper platform will likely be more difficult than if the platform were above the water. These considerations must be further investigated before designing a system for a large-scale pilot study.

Although both SMORE designs do not significantly affect the dynamics of the turbine to which they are attached, other considerations should be taken into account when selecting which SMORE design to deploy. Biofouling, which has been shown to have a detrimental effect on the adsorbent's uranium extract capabilities (Park et al., 2016), could be mitigated by submerging the upper platform as that may reduce light intensity, which is directly correlated to the growth of biological matter, at the adsorbent. The movement of water past the adsorbent's surface may also prevent biofouling as it creates a boundary layer within which it is hard for microorganisms to attach to the adsorbent thereby reducing the initial layer of biofouling. Specifically, research has also shown that there exists critical values of current speeds for different species of marine organisms above which fouling biomass is greatly reduced and in general fouling is not possible at speeds greater than 1.5 m/s (Railkin, 2003). Alternatively, UV light has been shown to have strong antibacterial properties (Lakretz et al., 2010) and thus adding UV LEDs to a point in the adsorbent net's path could also prevent the formation of biofilm and hence reduce biofouling. Moreover, submerging the upper platform to below the ocean surface could greatly reduce wave loads on the uranium harvester given that wave forcing decreases exponentially with depth. On the other hand, designing a chemical system to extract uranium from the adsorbent for SMORE with a submerged upper platform will likely be more difficult than if the platform were above the water. These considerations must be further investigated before designing a system for a large-scale pilot study.

ACKNOWLEDGMENTS

This work was supported by the U.S. Department of Energy Office of Nuclear Energy under Contracts No. DE-NE0008268, the National Academies Keck Futures Initiative, and the S.D. Bechtel, Jr. Foundation through the MIT Energy Initiative. This material is based upon work supported by the National Science Foundation Graduate Research Fellowship under Grant No. 1122374.Any opinion, findings, and conclusions or recommendations expressed in this material are those of the authors and do not necessarily reflect the views of the National Science Foundation.

REFERENCES

Byers, M F, Haji, M N, Slocum, A H, and Schneider, E (2016). "A Higher Fidelity Cost Analysis of Wind and Uranium from Seawater Acquisition symBiotic Infrastructure,"*In Proc. of the 2016 ANS Winter Meeting and Nucl. Tech. Expo*,Las Vegas, NV.

Chakrabarti, S K (1994). *Offshore Structure Modeling*, World Scientific, Singapore, SGP.

Haji, M N, Vitry, C, and Slocum, A H (2015). "Decoupling the functional requirements of an adsorbent for harvesting uranium from seawater through the use of shell enclosure,"*In Proc. of the 2015 ANS Winter Meeting and Nucl. Tech. Expo*, Washington, DC.

Haji, M N and Slocum, A H (2016). "Design of a Symbiotic Device to Harvest Uranium from Seawater through the use of Shell Enclosures,"*In Proc. of the 2016 ANS Winter Meeting and Nucl. Tech. Expo*, Las Vegas, NV.

Jonkman, J (2010). "Definition of the Floating System for Phase IV of OC3,"*Tech. Rep.*, NREL/TP-500-47535.

Jonkman, J, Butterfield, S, Musial, W, and Scott, G (2009). "Definition of a 5-MW reference wind turbine for offshore system development,"*Tech. Rep.*, NREL/TP-500-38060.

Jonkman, J and Matha, D (2009). "A Quantitative Comparison of the Responses of Three Floating Platforms,"*Conf. Rep.*, NREL/CP-46726.

Kim, J, Tsouris, C, Mayes, R T, Oyola, Y, Saito, T, et al., (2013). "Recovery of Uranium from Seawater: A Review of Current Status and Future Research Needs,"*Sep. Sci. Technol.*, 48(3), 367-387.

Kluger, J, Slocum, A H, and Sapsis, T P (2017). "A First-Order Dynamics and Cost Comparison of Wave Energy Converters Combined with Floating Wind Turbines,"*In Proc. of the Twenty-seventh (2017) International Ocean and Polar Eng. Conf.*, San Francisco, CA.

Lakretz, A, Ron, E Z, and Mamane H (2010). "Biofouling control in water by various UVC wavelengths and doses,"*Biofouling*, 26, 257–267.

Lee, C H, and Newman, J (2010). *WAMIT User Manual*, WAMIT, Inc., Chestnut Hill, MA.

Myhr, A, Bjerkseter, C, Ågotnes, A, and Nygaard, T A (2014). "Levelised cost of energy for offshore floating wind turbines in a life cycle perspective,"*Renewable Energy*, 66, 714–728.

Newman, J, and Sclavounos P (1988). "The computation of wave loads on large offshore structures,"*In Proc. of BOSS*.

OECD Nuclear Energy Agency (2016). "Uranium 2016: Resources, Production and Demand,"*Technical report*, OECD Nuclear Energy Agency and the International Atomic Energy Agency.

Oguma, K, Suzuki, T, and Saito, K (2011). "Determination of uranium in seawater by flow-injection preconcentration on dodecylamidoxime-impregnated resin and spectrophotometric detection,"*Talanta*, 84(5), 1209-1214.

Park, J, Gill, G A, Strivens, J E, Kuo, L-J, et al., (2016). "Effect Of Biofouling On The Performance Of Amidoxime-Based Polymeric Uranium Adsorbents,"*Ind. & Eng. Chem. Res.*, 55, 4328–4338.

Railkin, A I (2003). *Marine Biofouling: Colonization Processes and Defenses* CRC Press.

Schneider, E and Sachde, D (2013). "The Cost of Recovering Uranium from Seawater by a Braided Polymer Adsorbent System,"*Sci. Glob. Sec.*, 21(2), 134-163.

Sebastian, T and Lackner, M (2013). "Characterization of the unsteady aerodynamics of offshore floating wind turbines,"*Wind Energy*, 16, 339–352.

Seko, N, Katakai, A, Hasegawa, S, Tamada, M, Kasai, N, Takeda, H, Sugo, T and Saito, K (2003). "Aquaculture of uranium in seawater by a fabric-adsorbent submerged system, "*Nucl. Technol.*, 144(2), 274–278.

Tamada, M (2009). "Current status of technology for collection of uranium from seawater,"*Japan Atomic Energy Agency*.

Tran, T, and Kim, D (2015). "The platform pitching motion of floating offshore wind turbine: a preliminary unsteady aerodynamic analysis,"*J. of Wind Eng. and Ind. Aerodynamics*, 142, 65–81.